DNS OF COMPRESSIBLE PIPE FLOW EXITING INTO A COFLOW

Richard D. Sandberg, Neil D. Sandham
School of Engineering Sciences
University of Southampton
Southampton SO17 1BJ, UK
sandberg@soton.ac.uk, n.sandham@soton.ac.uk

Victoria Suponitsky
General Fusion Inc
108-3680 Bonneville Place, Burnbaby, BC V3N 4T5, Canada
v.suponitsky@soton.ac.uk

ABSTRACT

Direct numerical simulations were conducted of a fully turbulent canonical nozzle/jet configuration. For all cases, the target Reynolds number, based on the jet velocity and diameter, was specified as 7670 and the jet Mach number and coflow Mach number were varied. The effect of the nozzle lip on the turbulent flow exiting the nozzle was investigated, with particular emphasis on whether Reynolds stress profiles at the nozzle exit could be collapsed with profiles in the fully developed region, and whether local behaviour in the vicinity of the nozzle exit could be predicted using asymptotic theory. The DNS data were also used to investigate the effect of varying Mach number and coflow on the mean flow and whether the various flow cases could be collapsed using similarity arguments.

INTRODUCTION

Jet noise research over several decades has shown that several different sources contribute to the overall sound radiation from subsonic jets. These sources are: (i) large scale structures mainly occurring close to the potential core region, (ii) breakdown of large scale structures into fine-scale turbulence near the end of the potential core, (iii) fine-scale turbulence within the initial shear layers of fully turbulent jets, and (iv) trailing-edge noise resulting from the interaction between the flow and the solid wall at the nozzle exit.

The ultimate goal of this ongoing study is to perform direct noise computations, i.e. simulating directly both hydrodynamic and acoustic fields, that include *all* these sound sources. This requires the inclusion of the nozzle in the simulations, with a turbulent flow inside the nozzle. Furthermore, a large computational domain is necessary to capture the acoustic farfield. To simplify the problem we use a round pipe with sufficient length as a canonical nozzle. It was shown previously that a spatially developing pipe flow with sufficient streamwise length results in well defined turbulent upstream conditions suitable for direct noise computations of jets (Sandberg *et al.*, 2010).

For these spatially-developing pipe simulations it was found that the structure of the flow changed considerably when approaching the nozzle exit. The focus of the current paper is to investigate this near-nozzle behaviour, in particular the effect of the nozzle lip on the turbulent flow. Further, the effect of varying co-flow on the jet, especially on streamwise similarity, is investigated.

For round turbulent jets without coflow streamwise similarity of jets at various flow speeds was shown in Crow & Champagne (1971). However, a coflow with varying magnitude was specified for all DNS presented in the current work. In a study of coflowing jets, Nickels & Perry (1996) found that the excess velocity of the jet scales as the inverse of the streamwise coordinate, confirming earlier observations reported in Cantwell (1981). This behaviour was found upstream of the region where the asymptotic limit of the excess velocity being much smaller than the coflow magnitude is reached. All cases with different coflow values collapsed if the streamwise coordinate was scaled with the momentum radius. In the present contribution, we evaluate whether the data from the current DNS study shows the same behaviour.

NUMERICAL APPROACH

The compressible Navier–Stokes equations for the conservative variables are solved in cylindrical coordinates using a newly developed finite-difference DNS code. For the spatial discretization in the radial and streamwise directions a 4^{th}-order standard-difference scheme with Carpenter boundary stencils is applied. A spectral method using the FFTW3 library is used in the azimuthal direction, enabling an axis treatment that exploits parity conditions of individual Fourier modes. Time marching is achieved by an ultra low-storage 4^{th}-order Runge–Kutta scheme (Kennedy *et al.*, 2000). The stability of the code is enhanced by a skew-symmetric splitting of the nonlinear terms (Kennedy & Gruber, 2008) and by an 11 point wave-number optimized filter (Bogey *et al.*, 2009), used after each full Runge–Kutta cycle with a weighting of 0.2

Block	$L_z \times L_r$	$N_z \times N_r$	$Np_z \times Np_r$
1	50.0×1.0	624×68	48×4
2	110×1.0	2808×68	216×4
3	110×0.0416	2808×17	216×1
4	110×79.5	2808×833	216×49
5	50.5×79.5	624×833	48×49
total	N/A	3.14×10^6	14208

Table 1. Size, number of grid points and the number of processors for each block in the computational domain (see figure 1, left). All dimensions are normalized with R, where R is the radius of the pipe.

to remove grid-to-grid-point oscillations.

The computational domain comprises five blocks (see figure 1, top) which can be classified as subdomains containing: flow inside the pipe (block 1), jet development downstream of the pipe exit (blocks 2,3 and 4), and coflow and acoustic field upstream of the pipe exit (block 5). The size of each block along with the corresponding number of grid points and number of subdomains in the streamwise (z) and radial (r) directions is given in table 1. In the azimuthal direction 64 Fourier modes were employed (corresponding to 130 collocation points in physical space), resulting in a total of 408×10^6 grid points. The maximum gridspacing away from the jet exit (in both streamwise and radial directions) was chosen to resolve acoustic waves up to Strouhal number $St_D \approx 2$ (based on the jet velocity and diameter) with at least 10 grid points.

At the pipe inlet the mean streamwise velocity profile

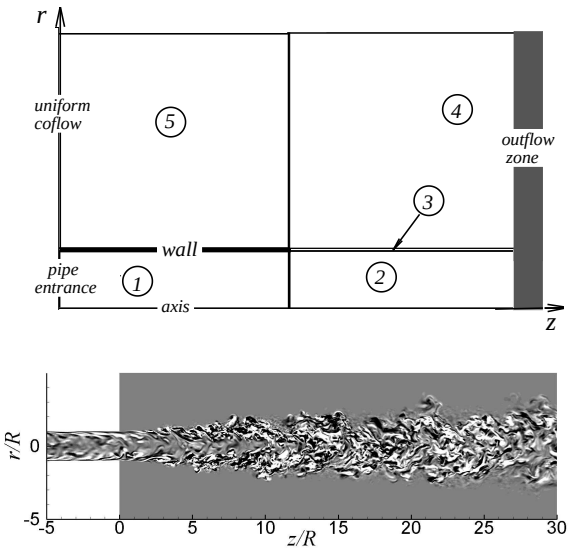

Figure 1. Sketch of the computational domain (top) and instantaneous contours of the azimuthal vorticity component, $M = 0.84$, $M_{co} = 0.2$ (bottom).

Case	M_{jet}	M_{co}	u_{co}	u_j	Re_{jet}
M84-c2	0.84	0.2	0.24	1.102	7,383
M64-c2	0.64	0.2	0.31	1.118	7,491
M46-c2	0.46	0.2	0.435	1.145	7,672
M46-c1	0.46	0.11	0.24	1.145	7,672

Table 2. Simulation parameters; M_{jet}, M_{co}, u_{co} and u_{jet} based on the bulk velocity in the nozzle, and Re_{jet} based on u_{jet} and nozzle diameter.

obtained from precursor periodic pipe calculations was prescribed, and the mean density and temperature profiles were set to be uniform. Turbulent fluctuations calculated using a digital filter technique (Touber & Sandham, 2009), using parameters also obtained from the periodic pipe simulations, were superposed onto the mean flow values. At the inflow boundary of block 5 a laminar boundary layer (Blasius solution) was prescribed with a boundary layer thickness $\delta/R = 0.0822$. At the outflow boundaries (blocks 2,3 and 4) a zonal characteristic boundary condition was applied (Sandberg & Sandham, 2006), while characteristic boundary conditions were used at the upper freestream boundary. It should be noted that while the thickness of the oncoming boundary layer as well as the thickness of the wall ($h_{wall} = 0.0468R$) were chosen arbitrarily, the ratio is $h_{wall}/\delta = 0.5695$, therefore a thin wall assumption is valid for our case. All simulations were run for a target Reynolds number of $Re_D = 6700$, based on the bulk velocity in the pipe and the diameter of the pipe, corresponding to $Re_{jet} = 7670$ when based on the jet velocity at the pipe exit.

More details on the length of the pipe needed to achieve fully developed flow and on the variation of pressure, density and temperature within the pipe for various nozzle Mach numbers are given in Sandberg *et al.* (2010).

RESULTS

Four DNS were conducted with the flow parameters listed in table 2. The simulations were run for at least 200 nondimensional time units (based on radius and bulk velocity inside the pipe) to allow the initial transients to leave the domain. All four cases were then continued for a further 600 to 800 time units to achieve statistical convergence.

In figure 1 (bottom), contours of the azimuthal vorticity component are shown for case M84-c2 to qualitatively illustrate the fully developed turbulent pipe flow exiting the nozzle and rapidly developing into a jet. It can be observed that the initial shear layers of the jet are already turbulent and do not undergo a laminar-turbulent transition.

Effect of nozzle exit on Reynolds stress components

The turbulent flow inside the nozzle was shown in Sandberg *et al.* (2010) to be axially independent from roughly 15 radii upstream of the nozzle exit onwards. It was also ob-

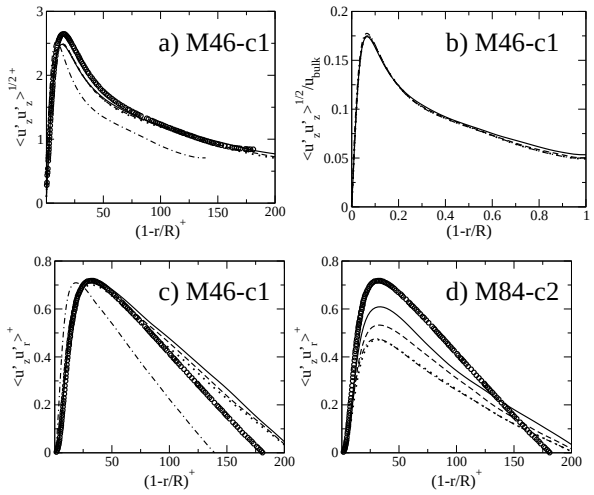

Figure 2. Axial turbulence intensity $< u_z' u_z' >^{1/2+}$ (a, b) and turbulence shear stress $< u_z' u_r' > /u_{bulk}^2$ (c, d) in wall coordinates (a, c, d) and outer coordinates (b) at various streamwise positions; (—) $z/R = -10$, (− − −) $z/R = -5$, (···) $z/R = -1$, (− · −) $z/R = 0$, (○) (Wu & Moin, 2008).

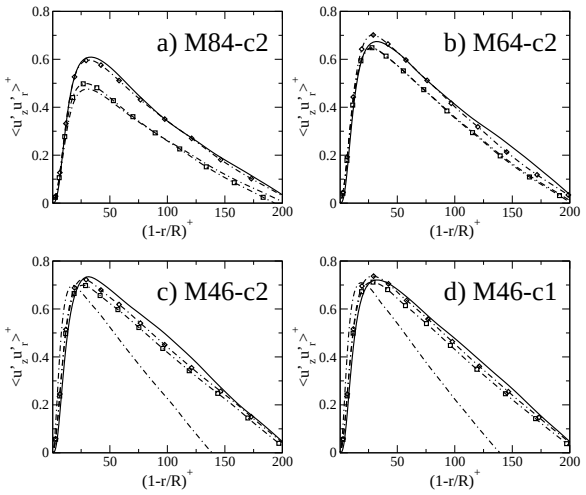

Figure 3. Turbulence shear stress $< u_z' u_r' >^+$ within nozzle in wall coordinates at various streamwise positions; (—) $z/R = -10$, (− · −) $z/R = 0$, (□) scaled with $(\partial u_z/\partial r)|_w$ from $z/R = -10$, (⋄) scaled with $(\partial u_z/\partial r)|_w$ and ρ_w from $z/R = -10$.

served that the Reynolds stress components in inner, or + coordinates, showed a considerable decrease in peak amplitudes approaching the nozzle exit. This behaviour is studied in more detail in the following.

Figures 2 (a, b) show the axial turbulence intensity for case M46-c1 in inner and outer coordinates at various streamwise positions. The profiles in outer coordinates are very similar at all streamwise locations, including at the nozzle exit $z/R = 0$. However, in inner (+) coordinates, data from all upstream locations appear to collapse to a fully developed profile that agrees well with the reference data of Wu & Moin (2008), while at the nozzle exit the axial turbulence intensity appears considerably reduced. The turbulence shear stress for case M46-c1 in wall coordinates (figure 2 c) also shows that the profiles within the fully developed region compare well with the incompressible reference data. The slightly larger value of the maximum $(1-r/R)^+$ and the resulting shallower slope compared with Wu & Moin (2008) is due to the slightly higher Reynolds number in the current study. However, at the nozzle exit, the shear stress profile is considerably altered. At the higher pipe Mach number of $M = 0.84$ (subfigure d) the shear stress profiles are seen to start reducing in amplitude already at $z/R = -5$ and the amplitude continues decreasing towards the nozzle exit.

The fact that the shear stress profiles change more visibly in plus coordinates than in outer coordinates, in particular for the low Mach number cases, suggests a change of the wall shear stress towards the nozzle exit. For inner scaling, the wall normal coordinate and the shear stress are scaled with u_τ/ν and u_τ^2, respectively, where $u_\tau^2 = \frac{\mu_{wall}}{\rho_{wall}} \left| \frac{\partial <u_z>}{\partial r} \right|_{r=1}$. For the current simulations, the pipe wall was considered isothermal, thus $\mu_{wall} = \text{const}$ and only ρ_{wall} and $\frac{\partial <u_z>}{\partial r}|_{r=1}$ can vary. To evaluate whether the change in wall shear stress is the main cause for the behaviour observed in figures 2 (c, d), the data obtained at $z/R = 0$ are scaled using i) the local values of ρ_{wall} and $\frac{\partial <u_z>}{\partial r}|_{r=1}$, or ii) the local value of ρ_{wall} and $\frac{\partial <u_z>}{\partial r}|_{r=1}$ from $z/R = -10$, or iii) ρ_{wall} and $\frac{\partial <u_z>}{\partial r}|_{r=1}$ from $z/R = -10$. Figure 3 shows that for the low Mach number cases, using the shear-stress value from upstream of the nozzle results in a collapse of the profiles obtained at the nozzle exit with data from the fully developed region. At the higher Mach number $M = 0.84$, using the wall-shear stress value from upstream does not suffice to recover the upstream turbulence shear-stress profile. Only when the wall density value from $z/R = -10$ is used in addition can the data obtained at the nozzle exit be collapsed with data from the fully developed region.

Being able to collapse the turbulence statistics at the nozzle exit with profiles in the fully developed region shows that the flow exiting the pipe can still be considered fully developed and therefore constitutes a well defined turbulent upstream condition suitable for direct noise computations.

Prediction of near-nozzle behaviour

The decrease in amplitude of turbulence statistics scaled by the wall shear stress at the pipe exit indicates an increase in skin friction towards the nozzle lip, consistent with analytic predictions using triple-deck theory (Stewartson, 1968; Messiter, 1970). The asymptotic solutions provided in the literature were derived for laminar boundary layers. However, it was shown in Sandberg & Sandham (2008) that the asymptotic scalings could produce results with reasonable accuracy for turbulent boundary layers when the eddy viscosity of the turbulence is accounted for. Here, the applicability of these results is evaluated for turbulent pipe flow exiting the nozzle. Stewartson (1968) derived the analytic expression for the skin friction in the immediate vicinity of the trailing edge (outer solution) as

$$c_f(z/R) = \frac{2\lambda}{Re_l^{1/2}} \left[1 + \Omega \left(\frac{l}{-\lambda^{1/2} Re_l^{3/4} z/R} \right)^{2/3} \right]$$

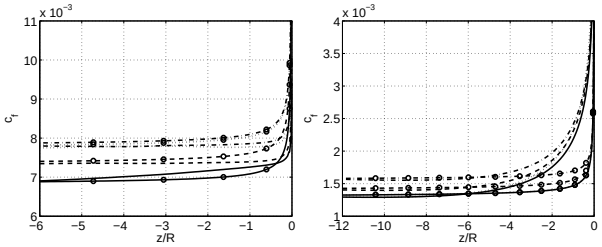

a) turbulent pipe b) coflow B-L

Figure 4. Time averaged skin friction coefficient c_f; lines denote results from simulations, lines with symbols denote solutions according to Stewartson (1968) (using the eddy viscosity correction for a); (—) M084-c2, (− − −) M064-c2, (− · −) M046-c2, (···) M046-c1.

$$\Omega = \frac{0.8966\Gamma(-1/3)\sqrt{3}}{2\pi}\,, \tag{1}$$

where $\lambda = 0.332$ and Re_l is the Reynolds number based on length of the surface, which in the current case was specified as the streamwise distance it would take to generate a boundary layer with thickness $\delta \sim 0.8R$.

To account for the turbulent nature of the present boundary layer, a simple correction was proposed in Sandberg & Sandham (2008). The eddy viscosity ν_T of the turbulent boundary layer can be estimated using Prandtl's mixing length theory, thus $\nu_T = \kappa(1-r/R)u_\tau$, with $\kappa = 0.41$. As the triple-deck solution is only valid very close to the wall, the eddy viscosity was evaluated at $(1-r/R)^+ = 20$ and assumed to be constant in the wall normal direction. To account for the turbulent viscosity the Reynolds number based on chord Re_l was divided by the ratio of eddy viscosity over molecular viscosity, which turns out to be close to the factor 2 for the present case.

The predictions obtained from (1) are compared to the DNS data for all cases in figure 4 a) and reasonable agreement is found both in terms of the onset of the increase and the amplitude reached at the nozzle exit. In addition to the turbulent flow inside the pipe, an attempt was also made to predict the behaviour of the laminar coflow boundary layer on the outer pipe wall close to the nozzle exit. Figure 4 b) shows a considerable difference between the predictions and the DNS data. Although the level of difference is surprising, it is consistent with the trend observed previously for flow over a flat plate trailing edge (Sandberg & Sandham, 2008). The disagreement between the DNS data and the theory for the laminar coflow was determined to be due to the pressure field being strongly modified by the Reynolds stress components of the turbulent pipe flow.

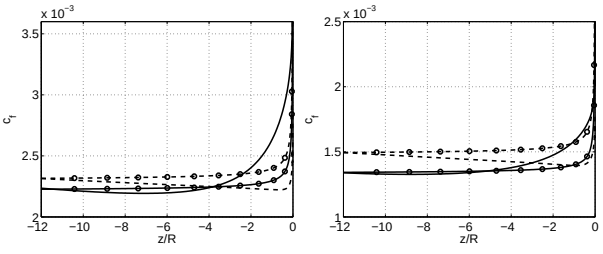

a) pipe (- -) and coflow (-) b) channel (- -) and coflow (-)

Figure 5. Skin friction coefficient c_f from laminar axisymmetric (a) and plane 2D (b) simulations for flow parameters according to case M46-c1; lines denote results from simulations, lines with symbols denote solutions according to Stewartson (1968).

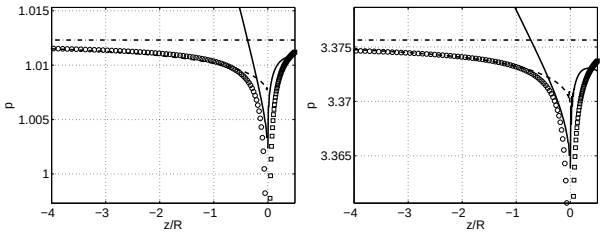

a) M84-c2, $c_1 = 1.2$ b) M46-c1, $c_1 = 0.4$

Figure 6. Mean pressure on the surface; (–) top surface, (- - -) bottom surface, $(-\cdot-)$ $p = 1/(\gamma M^2)$, symbols denote solutions according to Messiter (1970) using the eddy viscosity correction.

However, the current study considers a round geometry and is therefore fundamentally different from the trailing-edge case studied previously. To evaluate whether the additional radial terms in a round geometry are significant, two dimensional simulations of a pipe and a planar channel were conducted at the same flow conditions as case M46-c1. An effort was made to specify the coflow boundary layers such that their boundary layer thicknesses would be similar to the boundary layer on the pipe or channel walls in order to obtain roughly symmetric flow about the trailing edge as assumed in Stewartson (1968). The predictions shown in figure 5 still show considerable disagreement with DNS data, mainly in terms of the DNS data showing the skin friction increase confined to a much smaller streamwise extent than the predictions. It can also be observed that the increase in skin friction is limited to a significantly smaller streamwise extent on the inside of the wall, i.e. on the pipe/channel side, than on the coflow boundary layer side. It is suspected that this is due to the mean streamwise pressure gradient imposed on the channel or pipe flow. Nevertheless, it can also be concluded from the two dimensional cases that the effect of the radial terms on the near nozzle-exit region is negligible.

Messiter (1970) also provides an approximation to the pressure in the vicinity of the trailing edge, given as

$$p(z/R) = \begin{cases} \frac{1}{\gamma M^2}\left(1 - \frac{c_1 Re_l^{-1/2}}{3\sqrt{3}\sqrt{0.332}}(-z/R)^{-2/3}\right) & z/R < 0\,, \\ \frac{1}{\gamma M^2}\left(1 - \frac{c_1 Re_l^{-1/2}}{3\sqrt{3}\sqrt{0.332}}(z/R)^{-2/3}\right) & z/R > 0\,. \end{cases} \tag{2}$$

Figure 6 shows the asymptotic solutions of the mean pressure comparing well with the DNS results. The mean pressure decays towards the nozzle exit resulting in a favorable pressure gradient on the surface. The figures also highlight the large differences in mean pressure gradient between the inner (pipe) and outer (coflow boundary layer) walls.

Overall, these results suggest that the asymptotic solu-

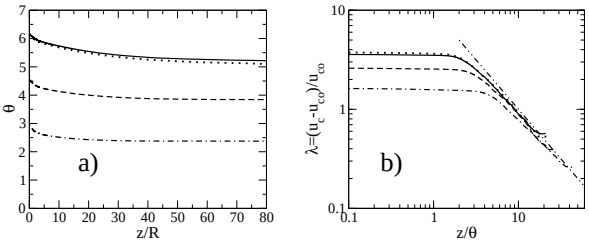

Figure 7. Momentum radius θ over streamwise coordinate (a) and excess velocity λ over streamwise coordinate scaled with momentum radius θ (b); (—) M084-c2, $(- - -)$ M064-c2, $(-\cdot-)$ M046-c2, $(\cdots)$ M046-c1, $(-\cdots-)$ $(z/R)^{-1}$.

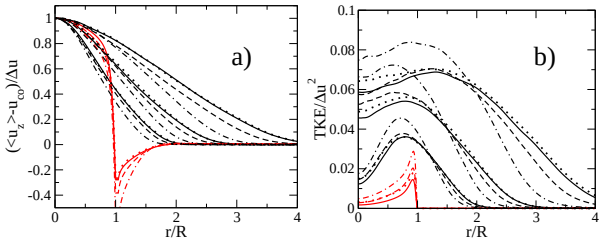

Figure 8. Time and azimuthally averaged streamwise velocity component (a) and turbulence kinetic energy (b) profiles over radial coordinate at streamwise positions $z/R = 0$, $z/R = 10$, $z/R = 20$, and $z/R = 40$; (—) M084-c2, $(- - -)$ M064-c2, $(-\cdot-)$ M046-c2, $(\cdots)$ M046-c1.

tions of Stewartson (1968) and Messiter (1970) are only qualitatively in agreement with the DNS data, with closest agreement observed for the fully turbulent pipe flow of the current canonical nozzle/jet configuration.

Jet similarity

All cases in the current study were conducted at roughly the same Reynolds number, based on the jet exit velocity and diameter. The parameters that were varied were the Mach numbers of the jets and the coflow Mach numbers. It was investigated whether the four different cases could be scaled such that quantities plotted over the streamwise coordinate or radial profiles at various streamwise locations could be collapsed. In an experimental study of coflowing turbulent jets by Nickels & Perry (1996), the excess velocity $\lambda = (u_c - u_{co})/u_{co}$ was shown to display a decay with z^{-1} downstream of the end of the potential core, as also reported in Cantwell (1981). Only considerably further downstream the asymptotic limit for coflowing jets of $z^{-2/3}$ was found, which is analogous to the defect velocity decay found for round wakes Cantwell (1981). Nickels & Perry (1996) were able to collapse the various coflow cases investigated by scaling the streamwise coordinate with the momentum radius θ, defined as

$$\rho u_{co}^2 \theta^2 = \int_0^\infty \rho < u_z > (< u_z > - u_{co}) 2\pi r dr \,, \text{or} \qquad (3)$$
$$\rho u_{co}^2 \theta^2 = 2\pi \left[\int_0^\infty \rho < u_z >^2 r dr - u_{co} \int_0^\infty \rho < u_z > r dr \right] .$$

The first term is the jet momentum flux, which is constant over z. However, the second term is the mass flux and can only be constant in the streamwise direction if there is no flux through the upper boundary. Thus, the overall momentum radius θ is only constant if entrainment can be excluded, as confirmed using data from the current cases shown in figure 7 a), where the computational domain is finite. In the experiments of Nickels & Perry (1996), considerable effort was spent to set up an experiment in which no boundary layers were generated on the outside of the nozzle. In the DNS, the flow exiting the nozzle has a fully developed pipe flow profile and the coflow develops a laminar boundary layer profile, as seen in figure 8 a). For the current case, the asymptotic values far downstream of the nozzle (at $z/R = 80$) were chosen to scale the streamwise coordinate and figure 7 b) illustrates that the excess velocities for most cases approach the correct slope downstream of the potential core. However, for the case M46-c2 the z^{-1} behaviour does not appear to be recovered exactly. In Nickels & Perry (1996) the asymptotic $z^{-2/3}$ behaviour was not reached until $z/\theta > 20$ which is further downstream than the outflow boundary in the current simulations and therefore cannot be investigated.

Figure 8 shows the radial profiles of the mean axial velocity component and the turbulence kinetic energy (TKE) at several streamwise locations. The velocity profiles have been scaled with the velocity difference $\Delta u = u_c - u_{co}$, with $u_c =< u_z > |_{r=0}$, and TKE is scaled with Δu^2 in an attempt to collapse the results from all cases. It appears that the profiles can be collapsed, except case M46-c2, for which not only the amplitudes deviate from the other cases, but also the shape of the profile does not resemble the data from the other cases, in particular for the TKE distribution.

It was also investigated whether the streamwise development of integral quantities, such as the momentum thickness, defined as

$$\delta_\theta = \frac{1}{R} \int_0^\infty \frac{< u_z > - u_{co}}{u_c} \left(1 - \frac{< u_z > - u_{co}}{u_c} \right) r dr \,, \qquad (4)$$

could be collapsed for all cases investigated. Downstream of the nozzle lip, the flow resembles a mixing-layer type flow, as seen in figure 8 a). Therefore, the streamwise derivative of the momentum thickness is expected to scale with the mixing layer parameter, defined here as $Q = (u_c - u_{co})/(u_c + u_{co})$. Figure 9 a) shows that the four cases can be collapsed reasonably well using this type of scaling. Further downstream, however, the flow transitions from a mixing-layer type to a jet with coflow type flow. From a turbulent spreading hypothesis one expects the streamwise derivative of δ_θ to be similar to $\Delta u/u_{conv}$, where u_{conv} is the eddy convection velocity. If one considers the flow far downstream of the nozzle, where the excess velocity becomes small compared with the coflow velocity, u_{conv} can be approximated with u_{co}. Figure 9 b) illustrates that all cases can be collapsed reasonably well up to $z/R \approx 40$, after which the M46-c2 case deviates significantly from the other cases.

Finally, the maximum value in the radial direction of fluctuating quantities such as TKE and pressure fluctuations

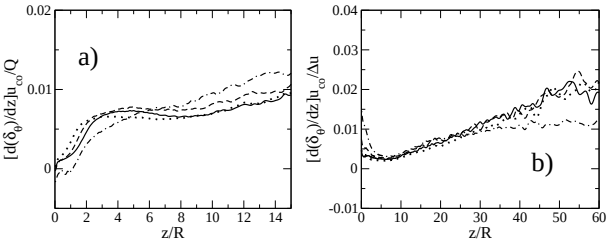

Figure 9. Streamwise derivative of momentum thickness $d\delta_\theta/dz$ scaled with Q (a) and $\Delta u/u_{co}$ (b) over streamwise coordinate; (—) M084-c2, (– – –) M064-c2, (– · –) M046-c2, (· · ·) M046-c1.

p_{rms}, which play a crucial role in the noise generation of the jets, were scaled with Δu^2 and are plotted over the streamwise coordinate in figure 10. A similar picture emerges as for the integral quantities discussed above, namely most cases can be collapsed reasonably well, except the M46-c2 case. Overall, these results suggest that the scalings applied here are applicable for small coflow velocities, but once a certain threshold ratio of coflow velocity to jet velocity is reached (in the case of the M46-c2 case, $u_{co}/u_{jet} \approx 38\%$), the flow becomes unique and cannot be collapsed with the other cases.

Conclusions

Direct numerical simulations of fully turbulent pipe flow exiting a nozzle and developing a turbulent jet were conducted. The jet Mach number and the coflow magnitude were varied at a constant target Reynolds number of $Re_{jet} = 7670$. It was shown that turbulence statistics at the nozzle exit could be collapsed with fully developed turbulent pipe flow profiles by using the wall shear-stress, and in the case of higher Mach number cases also the wall density, from the fully developed flow region upstream in the nozzle. This implies that the flow exiting the pipe can be considered fully developed and therefore constitutes a well defined turbulent upstream condition suitable for direct noise computations.

Comparison of predictions obtained from asymptotic theory with the DNS data showed only only qualitative agreement, with closest agreement observed for the fully turbulent pipe flow of the current canonical nozzle/jet configuration. It was demonstrated using 2D simulations that the cylindrical terms of the round jet case are negligible in the near-nozzle region.

It was found that the data from the different cases could be collapsed in the potential core region when scaling with the mixing layer parameter. Further downstream, the appropriate parameter was shown to be the velocity difference. However, the case with the highest coflow magnitude did not agree well with the other cases for any scaling used.

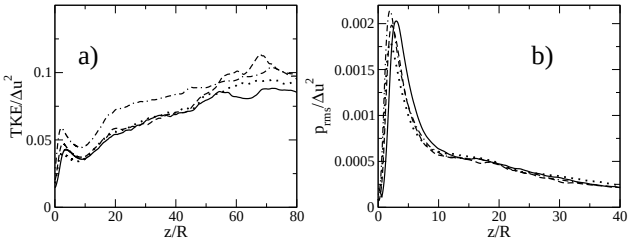

Figure 10. Maximum radial turbulence kinetic energy (a) and p_{rms} (b) over streamwise coordinate, scaled with Δu^2; (—) M084-c2, (– – –) M064-c2, (– · –) M046-c2, (· · ·) M046-c1.

This project was partly supported by the Royal Academy of Engineering/EPSRC research fellowship (EP/E504035/1) and computing time from EPSRC grant EP/G069581/1.

1 REFERENCES

BOGEY, C., DE CACQUERAY, N. & BAILLY, C. 2009 A shock-capturing methodology based on adaptative spatial filtering for high-order non-linear computations. *J. Comp. Phys.* **228** (5), 1447–1465.

CANTWELL, B. 1981 Organized motion in turbulent flow. *Annual Review of Fluid Mechanics* **13** (1), 457–515.

CROW, S. C. & CHAMPAGNE, F. H. 1971 Orderly structure in jet turbulence. *J. Fluid Mech.* **48**, 547–591.

KENNEDY, C., CARPENTER, M. & LEWIS, R. 2000 Low-storage, explicit Runge–Kutta schemes for the compressible Navier–Stokes equations. *Applied Numerical Mathematics* **35**, 177–219.

KENNEDY, C. & GRUBER, A. 2008 Reduced aliasing formulations of the convective terms within the Navier–Stokes equations for a compressible fluid. *J. Comp. Phys.* **227**, 1676–1700.

MESSITER, A. F. 1970 Boundary-layer flow near the trailing edge of a flat plate. *SIAM Journal on Applied Mathematics* **18** (1), 241–257.

NICKELS, T. & PERRY, A. 1996 An experimental and theoretical study of the turbulent coflowing jet. *J. Fluid Mech.* **309** (-1), 157–182.

SANDBERG, R., SUPONITSKY, V. & SANDHAM, N. 2010 DNS of a canonical compressible nozzle flow. *DLES 8* 8th Direct and Large-Eddy Simulation Workshop, Eindhoven, The Netherlands.

SANDBERG, R. D. & SANDHAM, N. D. 2006 Nonreflecting zonal characteristic boundary condition for direct numerical simulation of aerodynamic sound. *AIAA J.* **44** (2), 402–405.

SANDBERG, R. D. & SANDHAM, N. D. 2008 Direct numerical simulation of turbulent flow past a trailing edge and the associated noise generation. *J. Fluid Mech.* **596**, 353–385.

STEWARTSON, K. 1968 On the flow near the trailing edge of a flat plate. *Proceedings of the Royal Society of London, Series A: Mathematical and Physical Science* **306** (1486), 275–290.

TOUBER, E. & SANDHAM, N. 2009 Large-eddy simulation of low-frequency unsteadiness in a turbulent shock-induced separation bubble. *Theoretical and Computational Fluid Dynamics* **23** (2), 79–107.

WU, X. & MOIN, P. 2008 A direct numerical simulation study on the mean velocity characteristics in turbulent pipe flow. *J. Fluid Mech.* **608**, 81–112.